Isolated vs. Interconnected Wind Turbine Grounding Systems: Effect on the Harmonic Grounding Impedance, Ground Potential Rise and Step Voltage

Antonio Sunjerga[1], Quanxin Li[1,2], Dragan Poljak[3], Marcos Rubinstein[4], Farhad Rachidi[1]

[1] Electromagnetic Compatibility Laboratory, Swiss Federal Institute of Technology (EPFL), 1015 Lausanne, Switzerland

[2] School of Electrical Engineering, Wuhan University, Wuhan 430072, China

[3] Faculty of Electrical Engineering, Mechanical Engineering and Naval Architecture, University of Split, Split 21000, Croatia

[4] University of Applied Sciences of Western Switzerland (HES-SO), 1400 Yverdon-les-Bains, Switzerland

* Corresponding author. E-mail address: antonio.sunjerga@epfl.ch.

Abstract— Wind turbines are very vulnerable to lightning strikes due to their height, sharp edges and remote locations often with high soil resistivity. In this paper we present numerical simulations of the impedance of a typical wind turbine grounding geometry. We analyze the influence of interconnecting grounding systems of different wind turbines. IEC TR61400-24 suggests interconnection of grounding electrodes of wind turbines through horizontal electrodes (in the form of insulated or bare conductors) to achieve low steady-state grounding resistance. The analysis takes into account the frequency dependence of the soil electrical parameters. We show that the low frequency grounding impedance can be reduced by a factor of two or more as a result of interconnecting grounding systems. However, the reduction is significantly lower at higher frequencies because of the interconnection wire's inductance. We analyze the spatial distribution of the ground potential rise and step voltage in response to typical first and subsequent lightning return stroke current waveforms. It is shown that both, ground potential rise and step voltage can be significant along the wire, especially for high resistivity soil, and placing sensitive equipment near the interconnecting wire should be either avoided, or insulated wire should be used.

Index Terms—: Grounding impedance, wind turbine, interconnected, ground potential rise, step voltage, frequency dependent

1. Introduction

Damages to wind turbines caused by lightning strikes account for approximately 80% of wind turbine (WT) insurance claims [1]. Wind turbines are very vulnerable to lightning because of their height, sharp edges and remote and hilly locations often with low soil conductivity [2-4]. Tall structures not only attract downward discharges but, perhaps more importantly, they also initiate upward discharges [5]. There is some evidence that the probability of lightning incidence can be increased by the rotation of the blades [6]. Somewhere between 4% and 8% of wind turbines in Europe suffer damages due to lightning strikes each year [3].

The heights of wind turbines have been constantly increasing over the past years. As a result, they are more exposed to lightning and the design of a proper lightning protection system (LPS), which includes the grounding system, is of high importance. The lightning discharge current has a frequency spectrum ranging from DC up to a few MHz [7]. Proper grounding for the protection of the WT should be designed so that the impedance remains within acceptable limits. According to IEC, the grounding DC resistance should be preferably below 10 Ω [8].

IEC TR61400-24 [8] recommends interconnecting the grounding systems of adjacent wind turbines through horizontal electrodes (in the form of either insulated or bare conductors) to achieve low steady-state grounding resistance and to reduce interference injected into the electrical links. In the case of a single wind turbine, the length of horizontal wires used for impedance reduction is recommended to be limited to 80 m [8]. Of course, in the case of the interconnection of adjacent wind turbine grounding systems, the length of the cable will depend on the distance between the wind turbines and it can exceed the limit for individual turbines. The influence of an interconnecting wire has been analyzed in several studies [9-11]. In [9,11], beneficial effects of an interconnection in terms of the reduction of the early time response and the peak value of the grounding impedance have been observed. On the other hand, in [10], no significant difference was observed when adding an interconnecting wire, either connected or not to an adjacent wind turbine grounding system. This is probably due to the fact that the grounding system that was considered in [10,12] was significantly more extensive than those used in [9,11], so that the presence of an additional wire did not make any noteworthy effect.

In this paper, which is an extended version of the preliminary study presented in [13], we present numerical simulations for the impedance of a typical wind turbine grounding geometry. We also analyze the effects of interconnecting grounding systems of adjacent wind turbines. The presented analysis is based on a full-wave approach in which the frequency dependence of the soil parameters is taken into account. The influence of including the frequency dependence of the soil parameters has been considered in grounding analyses (e.g. [14,15]), but it has never been applied to the analysis of interconnected wind turbine grounding systems. Nonlinear effects associated with soil ionization [16] are expected to be significant only for peak currents higher than 100 kA and for very poorly conducting soils [17] and they are therefore disregarded in this study.

2. Geometry of problem

Typical grounding systems [18-20] consist of several rings connected with horizontal and vertical rods. The depth of the rings is usually a few meters and they are located within a foundation made of concrete [18]. Vertical or horizontal rods are often added to reduce the overall impedance. The effects of adding different rod geometries and the effect of additional rings are discussed in [19] and [20], respectively. The simplified geometry used in this paper is shown in Figure 1 while the related geometrical parameters are listed in Table 1. The geometry consists of 5 rings and four interconnecting wires. The current is injected into the center of the grounding system (origin of the coordinate system). Table 2 presents the electrical parameters of the soil for two different cases studied in this paper. It is worth noting that soil parameters are highly dependent on humidity [21,22] and this dependence can be expressed with empirical formulas (e.g., [23]).

We will consider the interconnection of two wind turbine grounding systems separated by 100 m (center to center) and connected with a 100-m long bare cable buried at a 1 m depth. All the wires are considered to be perfect electric conductors with 1-cm radius. The presence of concrete in the foundation has been disregarded by assuming that its parameters are the same as those of the surrounding medium (soil).

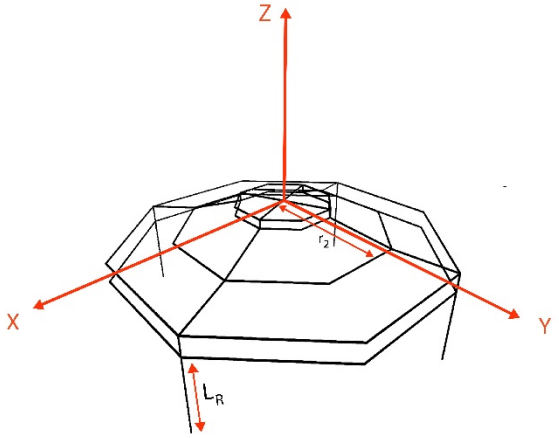

Fig. 1. Geometry of the simplified five rings grounding system configuration used in the study.

TABLE 1. Geometry of Model			
	r_i (m)	Z_i (m)	
Ring #1	2.6	-0.05	
Ring #2	2.6	-0.5	
Ring #3	5.8	-1.5	
Ring #4	9	-2	
Ring #5	9	-3	
	L_R(m)	Z_1 (m)	Z_2 (m)
Vertical rod	4	-3	-7

TABLE 2. Soil Parameters. ρ_{DC} and ε_∞ are the parameters of the frequency-dependent soil model given by equations (10) and (11).		
	ρ_{DC} (Ωm)	ε_∞
Case #1	1000	10
Case #2	100	10

3. Analysis Method

3.1 Full Wave Simulations

The full-wave calculations were carried out using the NEC-4 code, which is based on the numerical solution of the Pocklington integro-differential equation (for the case of wire structures) by means of the Method of Moments (MoM) [24]. A rigorous Sommerfeld integral approach was used in the evaluation of the current distribution. Once the current distribution is evaluated solving the Pocklington equation [25], the total electric field at an arbitrary point in space is calculated by summing the contributions of each wire segment.

The ground potential rise (GPR) at a given point on the ground surface can be evaluated as the line integral of the electric field:

$$V_{GPR}(x,y,f) = \int_{x,y\ z=0}^{x,y\ z=-\infty\ (remote\ earh)} \vec{E}(\vec{r},f)\cdot\overrightarrow{ds} \qquad (1)$$

The path to the remote earth is chosen vertically along the *z* direction to obtain faster convergence of the results. It is worth noting that the voltage is dependent on the chosen path at higher frequencies [26]. In this paper, the abbreviation GPR is used as the ground potential rise, also known as earth potential rise. This should not be confused with the grounding potential rise commonly referred to with the same GPR abbreviation (e.g. [27]), which relate only to the potential rise at the point of current injection and not at any arbitrary point on the ground surface.

The impedance of the grounding system can be calculated as

$$Z = \frac{V_{GPR}(x=0,y=0,f)}{I(f)} \qquad (2)$$

where $V_{GPR}(x=0,y=0,f)$ is the ground potential rise at the feeding point, and *I*(*f*) is the injected current.

3.2 Frequency Dependent Soil Parameters

There are several experimentally obtained formulas for modeling frequency dependence of the soil parameters. In this paper, we take into account the frequency dependent soil parameters in terms of the Smith and Longmire empirical formula [28], which is valid for the simulated frequency range (1 kHz to

10 MHz). The model of Smith-Longmire was selected essentially because of two reasons: (i) it provides results which are in good agreement with experimental results obtained by Bigelow and Eberle [29] and He et al. [30], and (ii) the equations satisfy causality [31]. Other models, such as the model of Messier [32] or that of Alipo and Visacro [33] could also have been used. According to Smith and Longmire, the soil parameters at a given frequency can be calculated using the following empirical formulas:

$$\varepsilon_R(f) = \varepsilon_\infty + \sum_{i=1}^{13} \frac{a_i}{1 + \left(\frac{f}{F_i}\right)^2} \tag{3}$$

$$\sigma(f) = \sigma_{DC} + 2\pi\varepsilon_0 \sum_{i=1}^{13} \frac{a_i F_i \left(\frac{f}{F_i}\right)^2}{1 + \left(\frac{f}{F_i}\right)^2} \tag{4}$$

where:

$$F_i = F(\sigma_{DC}) \cdot 10^{i-1} \tag{5}$$

$$F(\sigma_{DC}) = (125\sigma_{DC})^{0.8312} \tag{6}$$

and σ_{DC}=1/ρDC and ε_∞ are values of these parameters at zero frequency and asymptotic value at infinite frequency, respectively. The original expressions in [28] is adapted here in such a way that the input parameter is the DC conductivity instead of the moisture content.

The expressions for the coefficients a_i can be found in [31]. Figures 2 and 3 show the frequency dependence of the soil relative permittivity and resistivity for the two cases considered in Table 2. The implementation of this model is straightforward in the frequency domain. The NEC4 engine was embedded in MATLAB script, in which the soil parameters for each frequency step are calculated using (3)-(6) and used as input in NEC4.

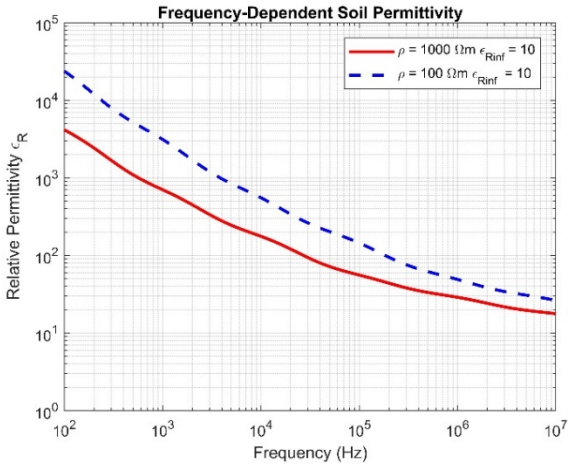

Fig. 2. Frequency-dependence of the soil relative permittivity. Case 1 (red solid line) and Case 2 (dashed blue).

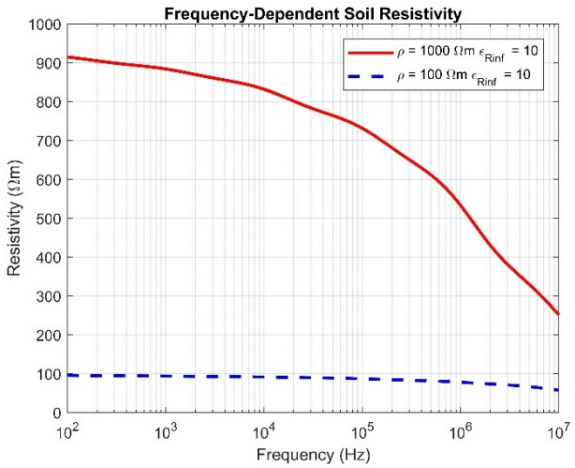

Fig. 3. Frequency-dependence of the soil resistivity. Case 1 (red solid line) and Case 2 (dashed blue).

3.3 Time-Domain Analysis

In order to evaluate the influence of the injected current waveform on the ground potential rise, two waveforms corresponding to typical first and subsequent return strokes were considered. The waveforms were represented using Heidler's functions, defined as [34]:

$$I_H(t) = \frac{I_0}{\eta} \frac{(\frac{t}{\tau_1})^n}{1 + (\frac{t}{\tau_1})^n} e^{-\frac{t}{\tau_2}} \tag{7}$$

where η can be calculated as:

$$\eta = e^{(-\frac{\tau_1}{\tau_2}(n\frac{\tau_2}{\tau_1})^{-n})} \tag{8}$$

The parameters of the Heidler's functions used to represent, respectively, a typical first return stroke and a typical subsequent return stroke are the same as those used in [35] and they are given in Table 3. The subsequent stroke is represented using the sum of two Heidler's functions. The early-time behavior of the two waveforms is shown in Fig. 4. The front time of the first and subsequent stroke are 4.125 μs and 0.5 μs respectively.

TABLE 3. Heidler's function parameters for the representation of typical first and subsequent return strokes (from [35])

	I_{01}(kA)	T_{11}(μs)	T_{21}(μs)	n_1	I_{02}(kA)	T_{12}(μs)	T_{22}(μs)	n_2
First Stroke	28	1.8	95	2	-	-	-	-
Subsequent stroke	10.7	0.25	2.5	2	6.5	2	230	2

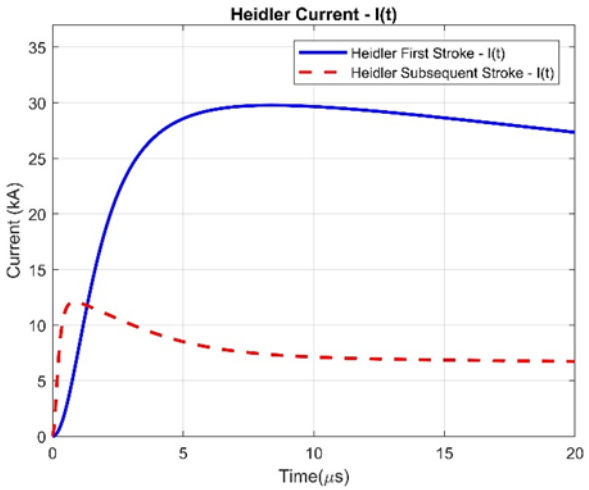

Fig. 4. Injected lightning current waveforms represented using Heidler's functions. First return stroke (solid blue); subsequent return stroke (dashed red)

The ground potential rise at a point (x, y) on the surface of the ground due to the first or the subsequent return stroke waveforms represented by the Heidler's functions is given by:

$$V_{GPR}(x, y, t) = \mathcal{F}^{-1}[Z_{tr}(x, y, f) I_H(f)] \qquad (9)$$

$I_H(f)$ is the injected current in frequency domain, $V_{GPR}(x, y, t)$ is the time-domain GPR at (x, y), and $Z_{tr}(x, y, f)$ is the transfer function determined as:

$$Z_{tr}(x, y) = \frac{V_{0\,GPR}(x, y, f)}{I_0(f)} \qquad (10)$$

in which $V_{0GPR}(x, y, f)$ is the response to a Dirac excitation current $I_0(f)$ (1 A at every frequency through the 1-MV voltage source in series with 1-MΩ impedance). The Inverse Fourier transforms are evaluated by way of the Inverse Fast Fourier Transform (IFFT) algorithm [36]. The transfer function is calculated at discrete frequencies from 1 kHz to 10 MHz with a non-uniform and adaptive sampling (more points in frequencies at which the transfer function changes more rapidly). The number of points varied from case to case with an average of about 80 points. Simulated impedances are interpolated using the Spline algorithm [37] to obtain a uniform frequency-domain sampling required for the IFFT algorithm.

4. Frequency-Domain Response

The effect of the frequency dependence of the soil parameters on grounding systems has been analyzed previously in frequency-domain simulations (e.g., [14] and [15] for the particular case of the grounding of wind turbines). On the other hand, the effect of interconnecting wind turbine grounding systems was analyzed using the finite-difference time-domain (FDTD) approach (e.g., [9, 10]) and in the frequency domain using the method of moments [11]. Here, we consider and discuss both of these effects for the same model solved in the frequency domain. It is worth noting that the three dimensional ground potential rise and step voltage have been reported only for the case of single wind turbines with constant soil parameters [19, 20].

First, we will examine the transient response of a single wind turbine grounding system. In a second case, we will analyze the effect of connecting the grounding system to that of an adjacent wind turbine using a 100-m long horizontal bare wire buried at 1 m depth. Finally, a third case will be examined, considering the grounding system and the 100-m long buried wire but without connection to the adjacent grounding system.
Figures 5 and 6 show the magnitude of the harmonic grounding impedance, respectively for the case of a high resistivity soil (Case #1) and a low resistivity soil (Case #2).
It can be seen that at low frequencies, the connection to an adjacent grounding system through a 100-m long wire results in a significant reduction of the harmonic grounding impedance. For higher frequencies (about 100 kHz for Case #1 and 10 kHz for Case #2), the effect of the adjacent grounding impedance becomes insignificant and the results for the grounding impedance of the whole system (WT connected to an adjacent one) coincide with those of a single WT with only the horizontal wire.

The influence of the connection wire can be understood intuitively from circuit theory. The current attenuation along the connecting wire is essentially due to:
(i) The leakage to the earth (conductance to remote earth), which results in the attenuation of the current along the wire. The lower the soil resistivity, the higher the attenuation.
(ii) The inductance of the wire, which is not significantly affected by the soil resistivity, and has an effect on the current as the frequency increases.
Considering the above, in the case of a low resistivity soil where the leakage is the main factor attenuating the current, the adjacent wind turbine grounding system becomes irrelevant, even at low frequencies. For

the case of a high resistivity soil, the connection to an adjacent wind turbine grounding system will be beneficial in reducing the grounding impedance at low frequencies, since both grounding systems can be considered to be in parallel. As the frequency increases, the impedance of the wire will also increase. This will result in reducing the effective length of the wire. As a result, a negligible current will reach adjacent wind turbine grounding.

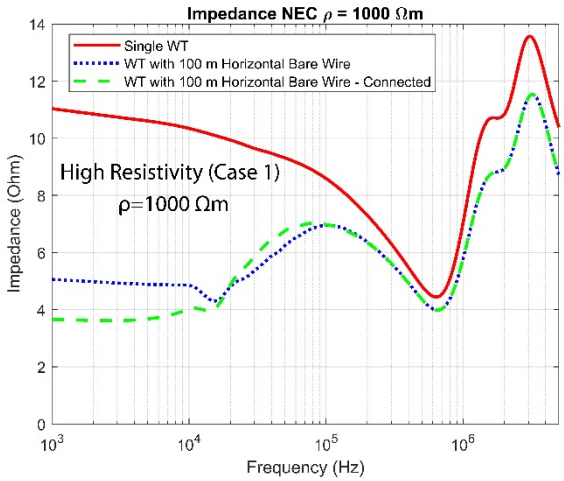

Fig. 5. Magnitude of the harmonic grounding impedance. Frequency-dependent soil parameters: ρ_{DC}=1000 Ωm, ε_{∞}=10. Single WT (solid red), WT with 100-m long buried horizontal wire (dotted blue) and WT with 100-m long buried horizontal wire connected to an adjacent grounding system (dashed green).

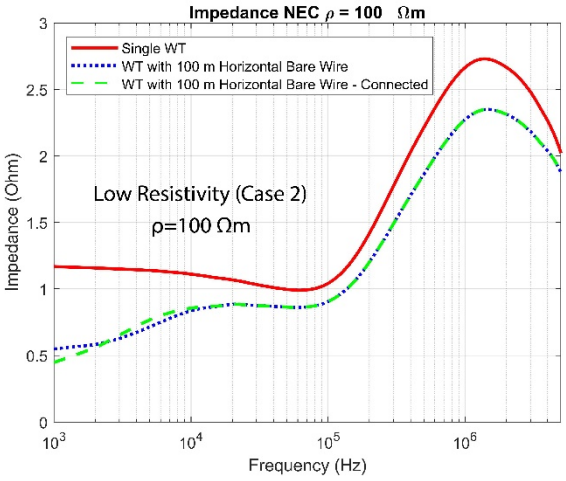

Fig. 6. Magnitude of the harmonic grounding impedance. Frequency-dependent soil parameters: ρ_{DC}=100 Ωm, ε_{∞}=10. Single WT (solid red), WT with 100-m long buried horizontal wire (dotted blue) and WT with 100-m long buried horizontal wire connected to an adjacent grounding system (dashed green).

In Fig. 7, we compare the results assuming constant soil parameters versus frequency-dependent soil parameters, for a single WT (Fig. 7a), and for two interconnected WTs using a 100-m long bare wire (Fig. 7b). The results are presented for the case of a high ground resistivity (ρ_{DC}=1000 Ωm), for which the effect of the soil frequency-dependent parameters is more significant on the grounding impedance. We can see that the frequency dependence of the soil electrical parameters affects the grounding impedance over the whole frequency range in both cases. At very low frequencies, there is no displacement current and the impedance is only governed by the soil resistivity and not the permittivity. As the frequency goes to zero, the soil resistivity becomes the same for both models (eq. 4). For example, at 100 Hz in the case of Fig. 7a and Fig. 7b, the models converge to 12.49 Ω and 4.18 Ω, respectively.

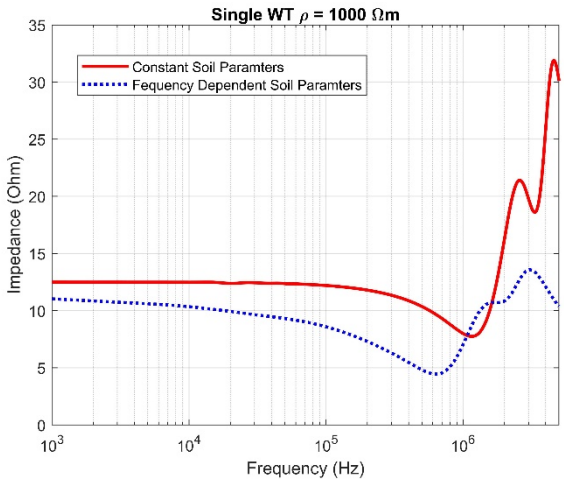

(a)

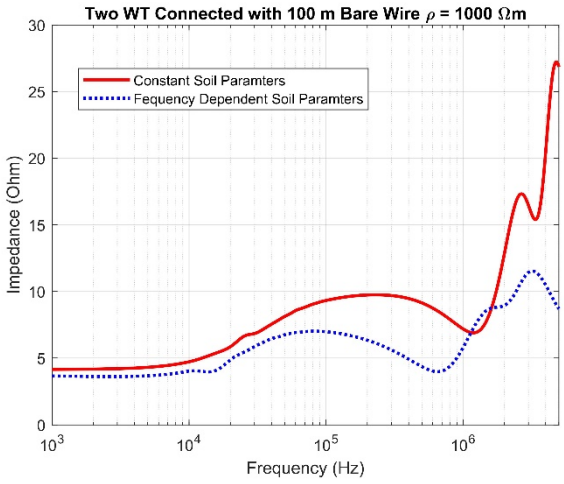

(b)

Fig. 7. Magnitude of the harmonic grounding impedance for the case of high resistivity soil ρ_{DC}=1000 Ωm, ε_∞=10. Constant soil parameters (solid red), frequency dependent parameters (dashed blue). (a) Single WT, (b) Two WT connected with a 100-m bare wire.

5. Time Domain

In this Section, we will examine the GPR time evolution and spatial distribution as well as the step voltage spatial distribution for the two considered cases of soil resistivity, and for the first and subsequent stroke waveforms. As in the previous section, we will consider the cases of a single WT, a WT with a 100-m long bare wire, and two WTs connected with a 100-m long bare wire. We show the spatial distribution of GPR and step voltage at the time instant of its maximum. The full spatial time evolution can be seen in the attached animations.

5.1. Time Evolution of the Ground Potential Rise

In this section, we present the time evolution of the GPR at specific locations along the axis perpendicular to the interconnecting wire and horizontal.
Figs. 8 and 9 present the ground potential rise for the case of high and low resistivity soils, respectively. The time evolution is plotted at four different points, including the current injection point at the origin of the coordinate system (x=0, y=0). and at distances of 4, 8 and 10 meters away in the direction perpendicular to the connecting wire. As expected, moving away from the injection point, we observe a decrease of the potential. The observed waveforms are qualitatively in agreement with the results of Yamamoto et al. [12,38], having in mind the differences in the considered geometries and adopted

models. In [12,38], the multi-layer soil model results in the appearance of reflections in the voltage waveform. In [38], the measured peak GPR values are lower than the simulated ones by a few tens of percent. This might be due to the fact that the simulations presented in [38] are based on the assumption of constant soil parameters. In both considered soil resistivity cases, a decrease of the peak GPR is observed for the case when an interconnected wire is used, whether alone or connected to an adjacent WT grounding system. It can be seen that the decrease of the peak value is only due to the interconnecting wire. The adjacent WT grounding system will only decrease the late-time response in the case of a high resistivity soil, in agreement with what was observed in the previous section in the frequency domain.

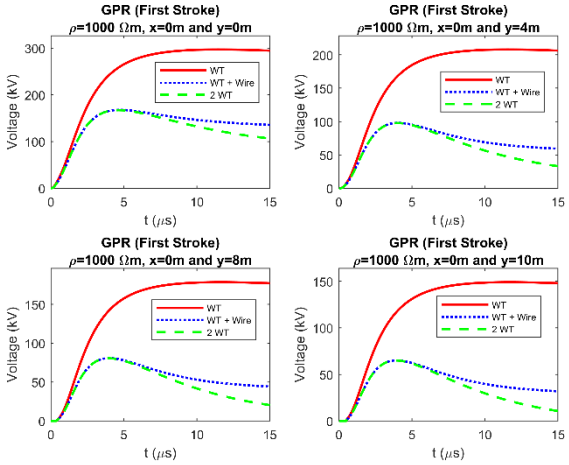

(a)

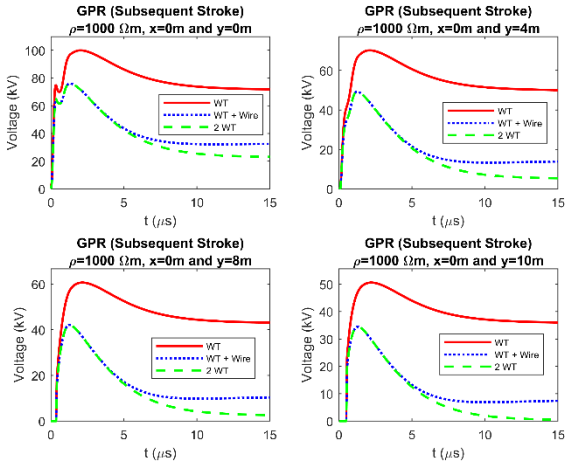

(b)

Fig. 8. Time evolution of the ground potential rise for the case of high resistivity soil and for the three considered geometries: Single WT (solid red), WT with a 100-m long buried horizontal wire (dotted blue), and WT with a 100-m long buried horizontal wire connected to an adjacent grounding system (dashed green). (a) First stroke, (b) Subsequent stroke.

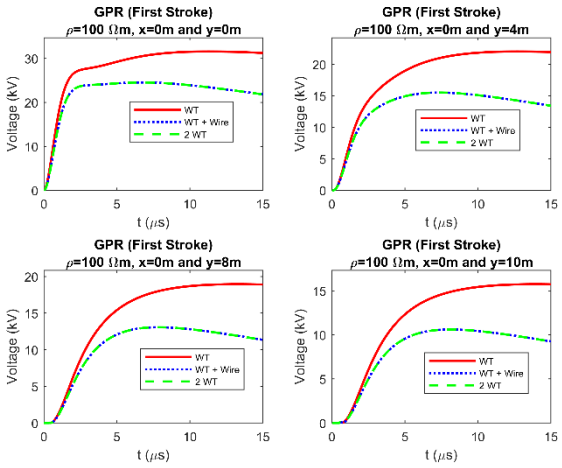

(a)

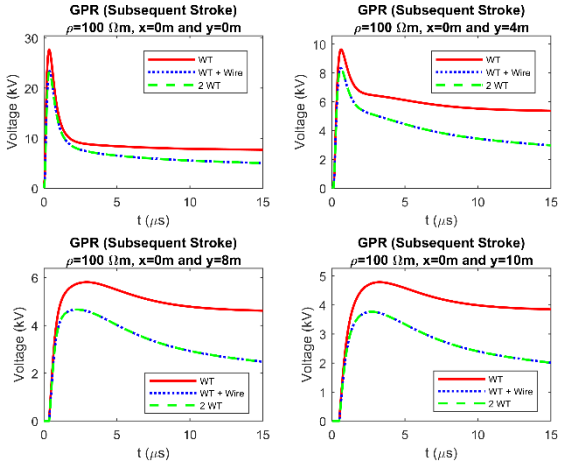

(b)

Fig. 9. Time evolution of the ground potential rise for the case of low resistivity soil and for the three considered geometries: Single WT (solid red), WT with a 100-m long buried horizontal wire (dotted blue), and WT with a 100-m long buried horizontal wire connected to an adjacent grounding system (dashed green). (a) First stroke, (b) Subsequent stroke.

5.2 Spatial Distribution of the Ground Potential Rise

Figures 10 and 11 show the ground potential rise for the case of a high resistivity soil with a single WT grounding, and a system of two WT groundings separated by 100 m and connected with bare wire, respectively. We can see that the connection to an additional WT leads to a maximum GPR that is significantly reduced and that it occurs much earlier in time. On the other hand, the level of GPR along the connecting wire in Figure 9 is significant and comparable to the maximum level at the feeding point. Figures 12 and 13 show the GPR for the case of a low resistivity soil. Again, it can be seen that the interconnection of the grounding systems results in an overall reduction of the GPR. Furthermore, it can be seen that the maximum GPR at the feeding point occurs at an earlier time compared to the case of a highly resistive soil.

The GPR reduction as a result of interconnecting grounding systems is more significant for first return strokes (characterized by slower waveforms) compared to subsequent return strokes. In the case of a low resistivity soil, the GPR is, as expected, more localized around the grounding center.

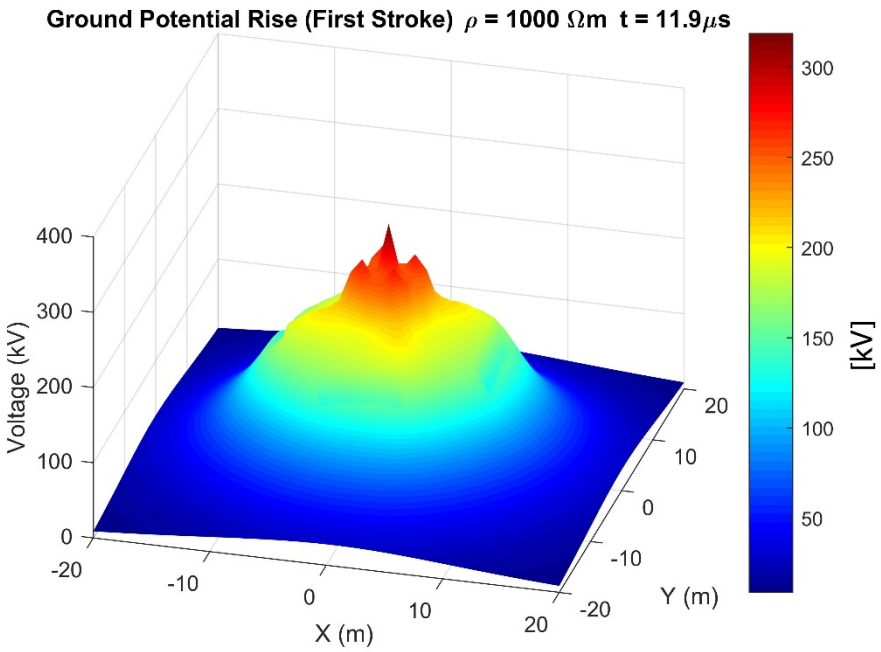

(a)

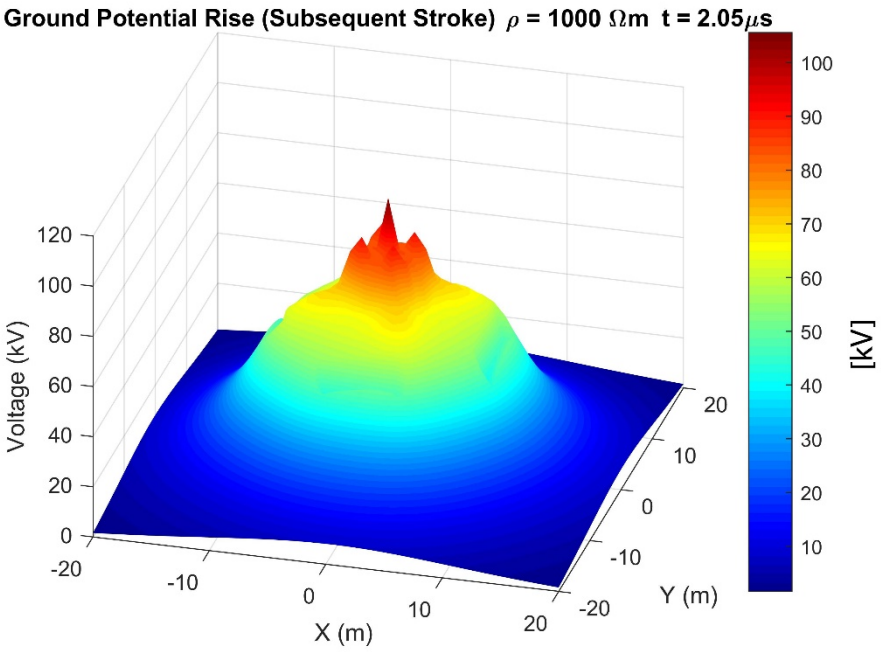

(b)

Fig. 10. Ground potential rise for single wind turbine grounding at the time when it attains its maximum at the feeding point. Case #1, ρ_{DC}=1000 Ωm. (a) First stroke, (b) subsequent stroke.

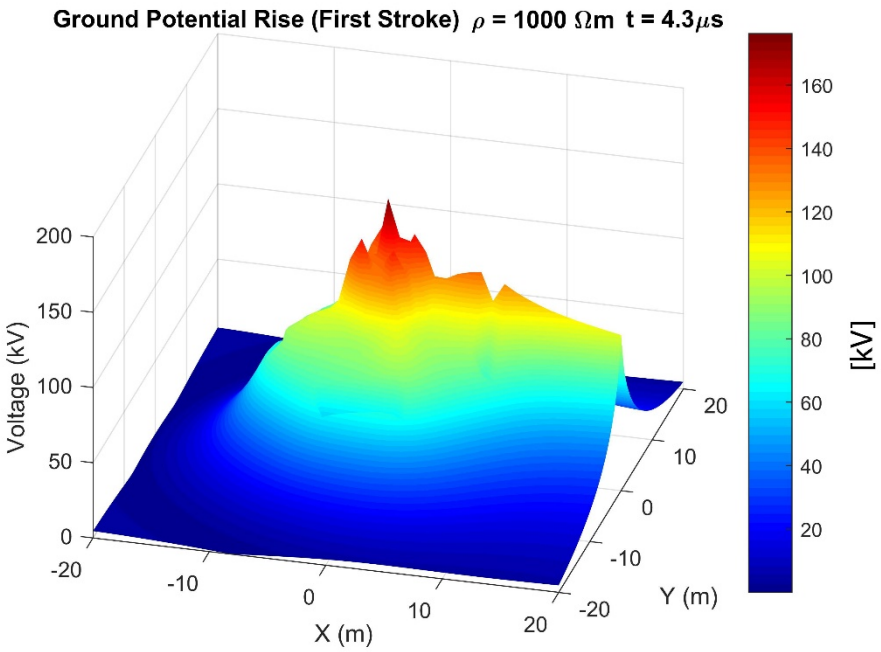

(a)

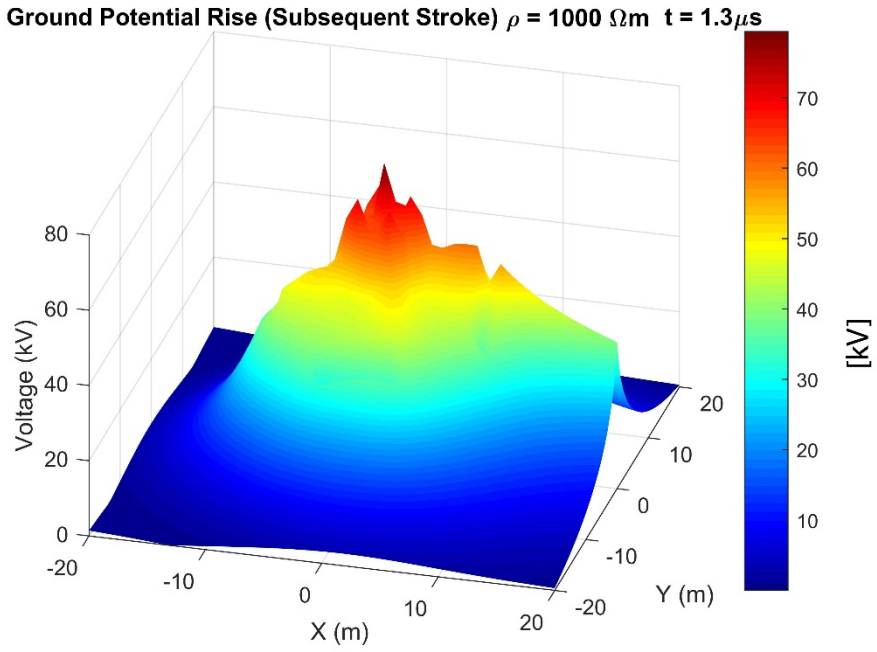

(b)

Fig. 11. Ground potential rise at the time when the maximum value is attained at the feeding point for two 100-m separated wind turbine groundings connected with 100 m of bare wire. Case #1, ρ_{DC}=1000 Ωm. (a) First stroke, (b) subsequent stroke.

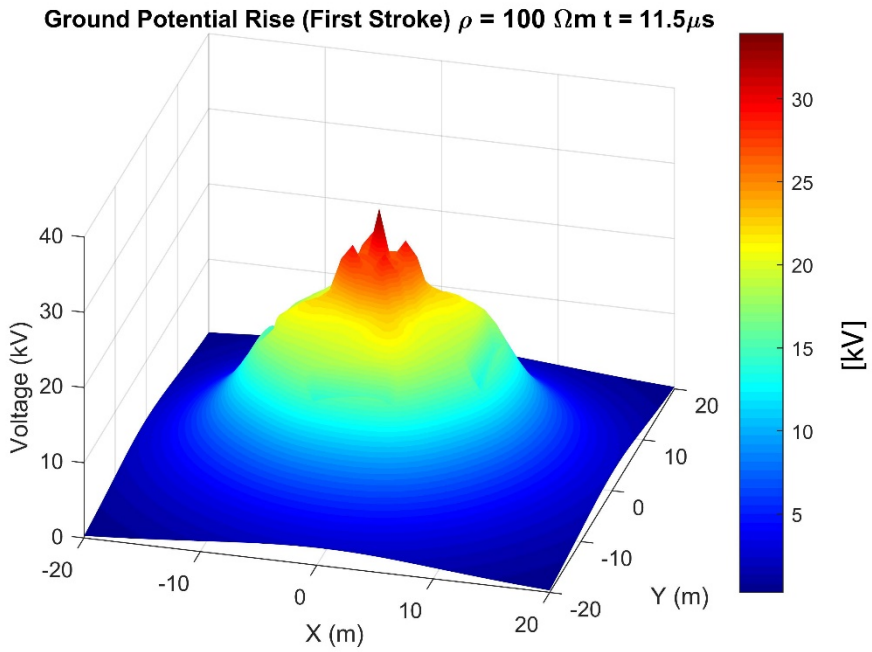

(a)

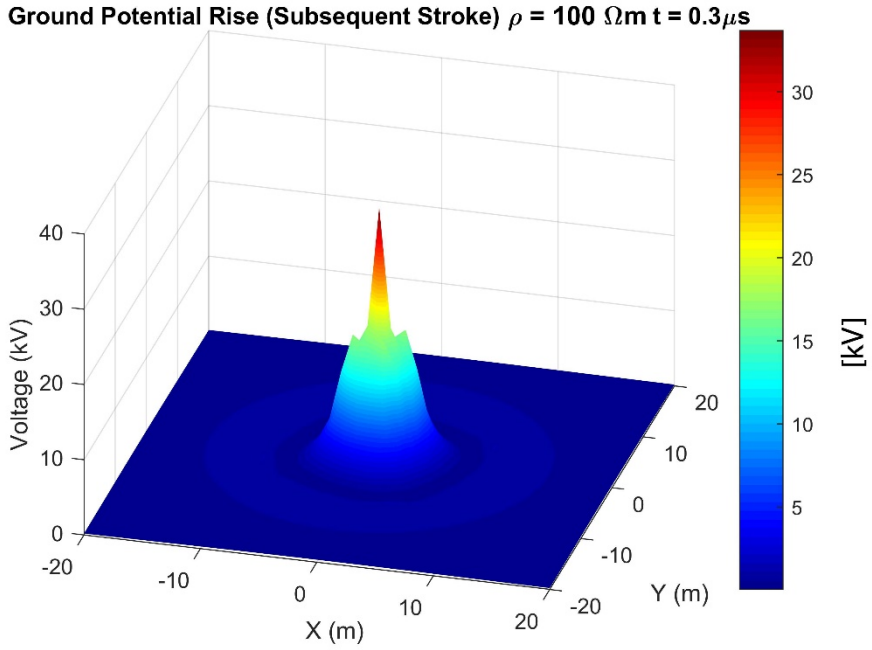

(b)

Fig. 12. Ground potential rise for single wind turbine grounding at the time when the maximum value is reached at the feeding point. Case #2, ρ_{DC}=100 Ωm. (a) First stroke, (b) subsequent stroke.

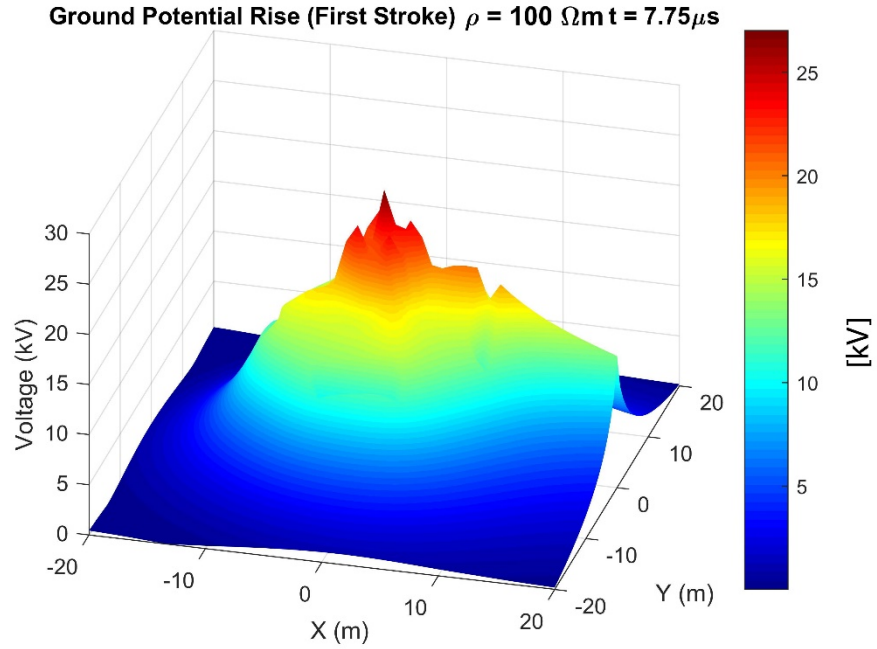

(a)

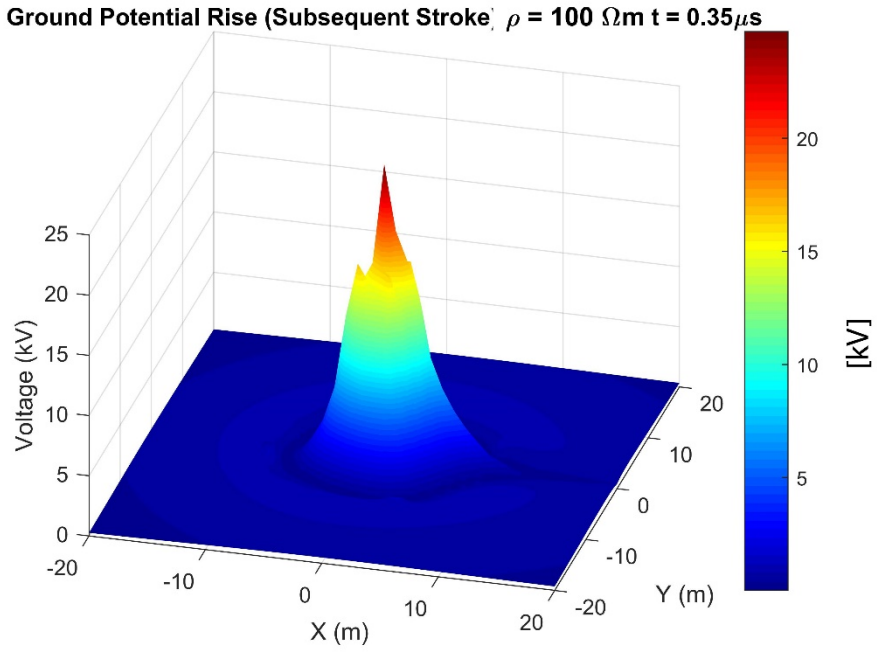

(b)

Fig. 13. Ground potential rise at the time when the maximum is reached at the feeding point for two 100m separated wind turbine grounding connected with 100m bare wire. Case #2, ρ_{DC}=100 Ωm. (a) First stroke, (b) subsequent stroke.

5.3 Step Voltage

The step voltage is calculated as a potential difference between two points on the earth surface at a distance of 1 m. Figures 14 and 15 show the step voltage for the case of high resistivity soil with a single WT grounding, and two WT grounding systems connected with a 100-m long bare wire, respectively. Similar to the GPR, we can see that for interconnected WT grounding systems, the maximum step voltage is significantly reduced and it occurs much earlier. However, the step voltage along the connecting wire and at location of vertical rods can be significant and comparable to the maximum level at the feeding point.

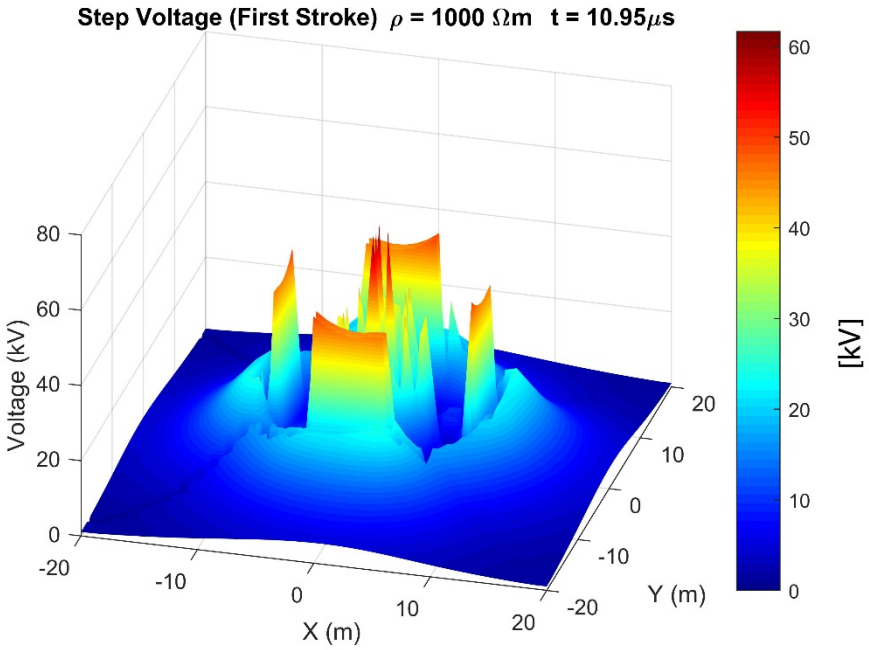

(a)

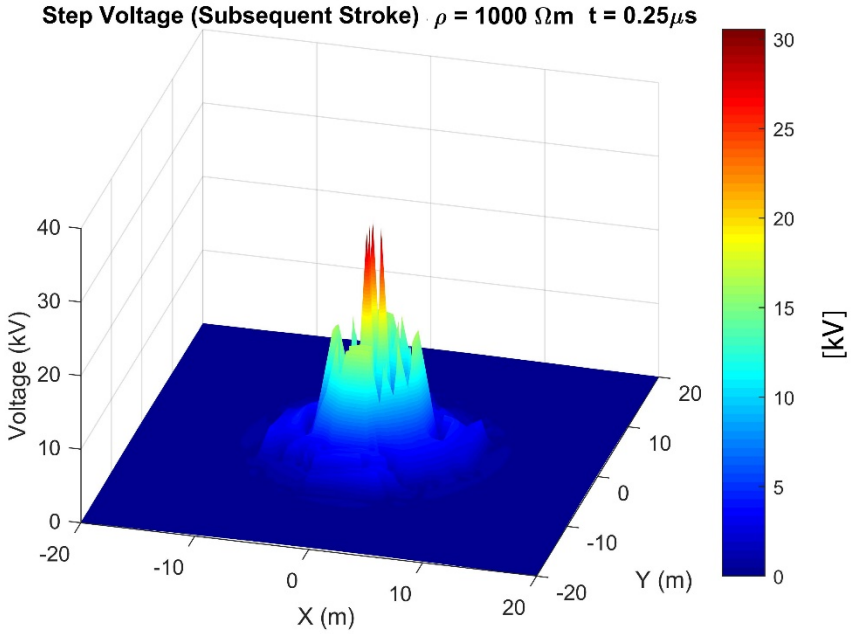

(b)

Fig. 14. Step voltage for a single wind turbine grounding at the time when the maximum is reached at the feeding point. Case #1, ρ_{DC}=1000 Ωm. (a) First stroke. (b) subsequent stroke.

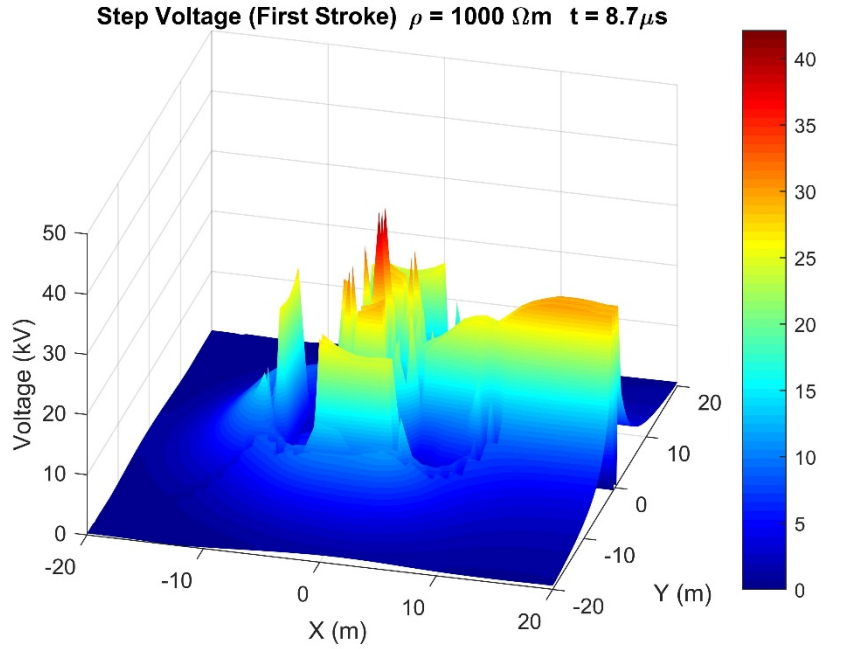

(a)

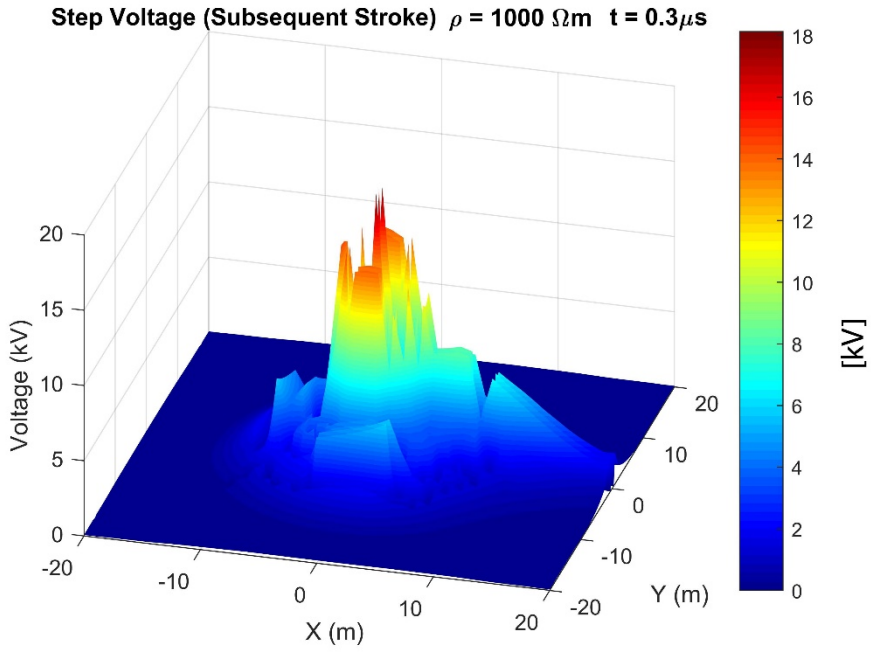

(b)

Fig. 15. Step voltage at the time when the maximum is reached at the feeding point for two 100-m separated wind turbine groundings connected with a 100-m bare wire. Case #1, ρ_{DC}=1000 Ωm. (a) First stroke. (b) subsequent stroke.

Figures 16 and 17 show the step voltage for the case of a low resistivity soil. Again, it can be seen that the interconnection of grounding systems results in the reduction of the overall step voltage. However, in this case, and unlike the case of a highly resistive soil, the step voltage along the interconnecting wire is much smaller compared it to the maximum at the feeding point.

The step voltage reduction as a result of interconnecting grounding systems is more significant for first return strokes (characterized by slower waveforms) compared to subsequent return strokes. In the case of a low resistivity soil, as expected, the step voltage is more localized around the grounding center.

The step voltage along the wire is less significant in case of low resistivity, but it is comparable to the maximum value at late times (see attached animation).

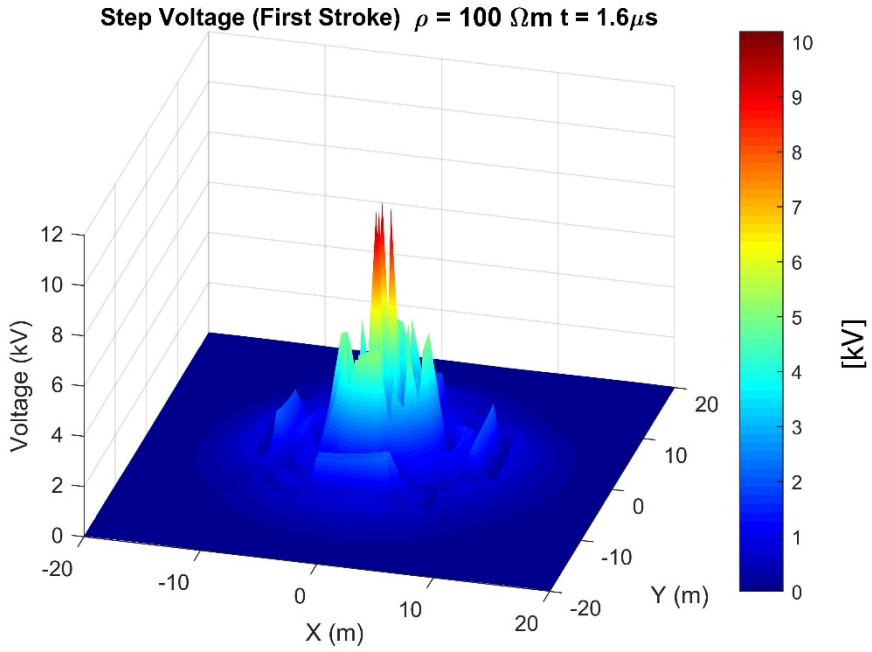

(a)

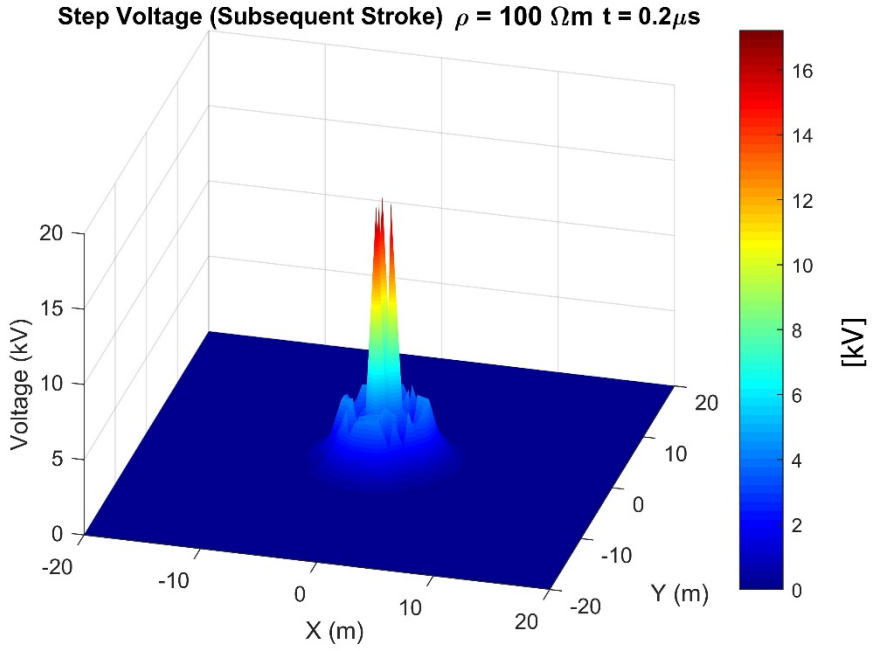

(b)

Fig. 16. Step voltage for single wind turbine grounding at the time when the maximum is reached at the feeding point . Case #2, ρ_{DC}=100 Ωm. (a) First stroke. (b) subsequent stroke.

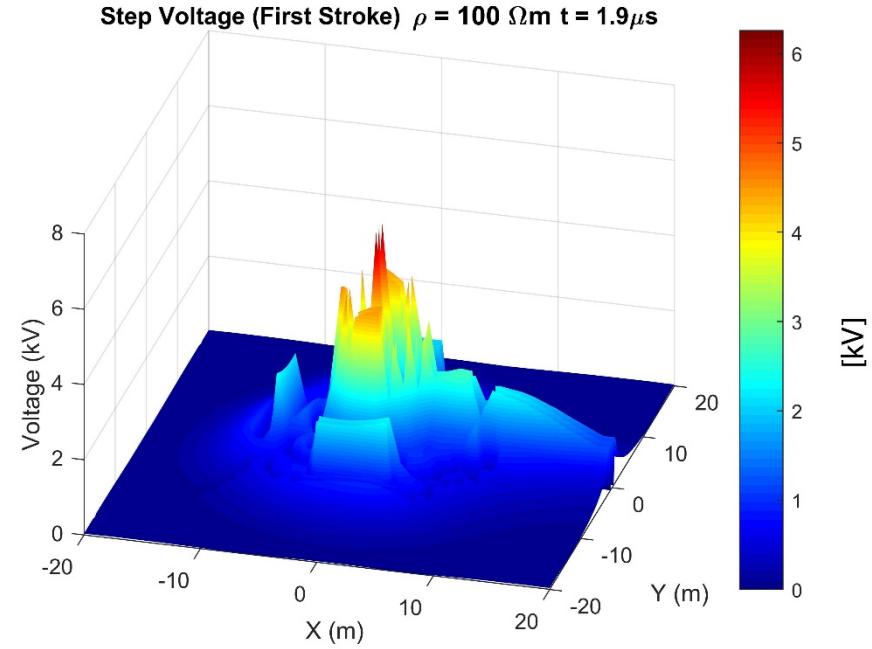

(a)

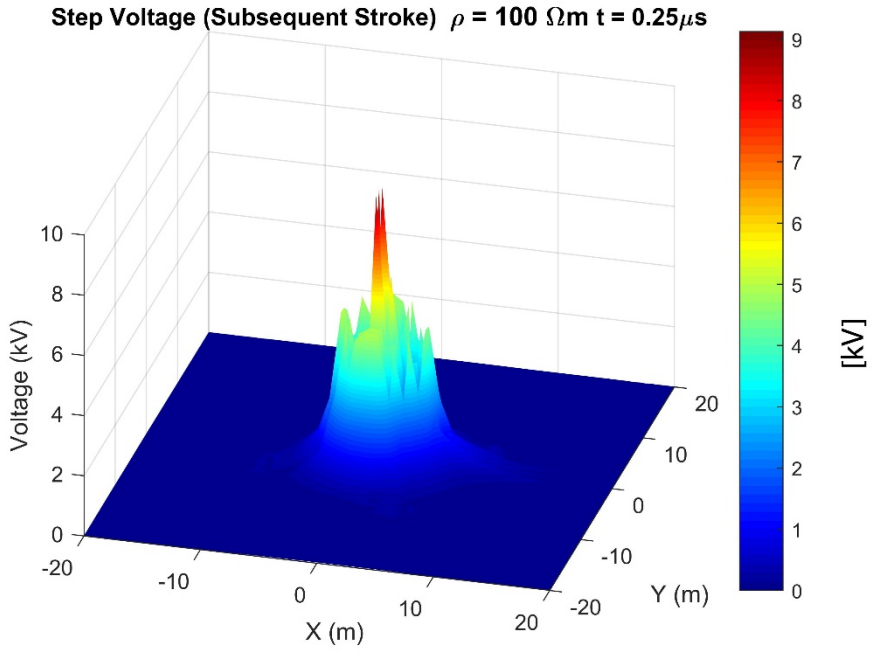

(b)

Fig. 17. Step voltage at the time when the maximum is reached at the feeding point for two 100-m separated wind turbine grounding connected with a 100-m bare wire. Case #2, ρ_{DC}=100 Ωm . (a) First stroke. (b) subsequent stroke

6. Conclusions

We presented numerical simulations for the impedance of a typical wind turbine grounding geometry, focusing on the effect of interconnecting grounding systems for different wind turbines, as recommended by IEC (TR61400-24). In the case of a single wind turbine, the length of horizontal wires used for impedance reduction is recommended by IEC to be limited to 80 m. Modern wind turbines have blades with lengths of 60 m and longer. Therefore, the distance between adjacent wind turbines is in practice much higher than 80 m. The analysis accounts for the frequency dependent soil electrical parameters.

It was shown that the low frequency grounding impedance could be reduced by a factor of two or more as a result of interconnecting two grounding systems separated by a 100-m distance. However, the reduction is significantly lower at higher frequencies due to influence of the interconnecting wire's inductance.

The results of this study show that the reduction of the GPR peak values in interconnected WTs is essentially due to the interconnecting wire. Adjacent wind turbines can only reduce the late-time response for the case of low resistivity soils since, in the early time, the effective length of the interconnecting wire is lower than the typical distance between wind turbines.

We analyzed the spatial distribution of ground potential rise and the step voltage in response to typical first and subsequent lightning return stroke current waveforms. We showed that both, the ground potential rise and the step voltage could be significant along the wire, in particular for the highly resistive soil. We also observed a high step voltage at locations of vertical rods that are a potential risk to the personnel. Furthermore, placing of sensitive equipment near the interconnecting wire should be either avoided, or insulated wire should be used.

Future work will include the taking into account of the presence of concrete in the foundation of the wind turbine.

7. Acknowledgment

Special thanks to four anonymous reviewers whose constructive comments improved this paper. This work was supported in part by the Swiss National Science Foundation (Project No. 200020_175594).

8. References

[1] D. I. B. Djalel, M. Mourad, and S. Ghoudelbourk, "Protection of wind turbine against the lightning damage," in IREC2015 The Sixth International Renewable Energy Congress, 2015.
[2] D. Poljak, D. Čavka, Properties and Characterization of Modern Materials, Chapter Electromagnetic Compatibility Aspects of Wind Turbine Analysis and Design July 2016.
[3] F. Rachidi, M. Rubinstein, J. Montanyà, J. Bermúdez, R.Sola, G. Solà, and N. Korovkin, "A Review of Current Issues in Lightning Protection of New-Generation Wind-Turbine Blades", IEEE Transactions on Industrial Electronics, Vol. 55, No. 6, June 2008.
[4] A. Sunjerga, F. Rachidi, M. Rubinstein, and D. Poljak, "Calculation of the Grounding Resistance of Structures Located on Elevated Terrain," IEEE Transactions on Electromagnetic Compatibility, pp. 1–5, 2018.
[5] F. Rachidi, M. Rubinstein and A. Smorgonskiy, Lightning Protection of Large Wind-Turbine Blades, in Wind Energy Conversion Systems, Springer, p. 227-242, 2012.
[6] "Turbines shoot upside-down lightning," Nature, vol. 506, no. 7488, pp. 268–268, Feb. 2014.
[7] CIGRE Working Group C4.407 (Convener: V.A. Rakov), "Lightning Parameters for Engineering Applications", Technical Brochure 549, CIGRE, 2014.
[8] IEC International Standard. Lightning protection. IEC 61400e61424. In: Wind turbine generation system, vol. 24. Geneva: International Electro-technical Commission; 2010.
[9] M. R. Ahmed and M. Ishii, "Effectiveness of interconnection of wind turbine grounding influenced by interconnection wire," in 2012 International Conference on Lightning Protection (ICLP), 2012.
[10] J. Niihara, A. Ametani, and K. Yamamoto, "Transient grounding characteristics of wind turbine with counterpoise," in 2012 Asia-Pacific Symposium on Electromagnetic Compatibility, 2012.
[11] B. Markovski, "Transient performance of interconnected wind turbine grounding systems," PRZEGLĄD ELEKTROTECHNICZNY, vol. 1, no. 6, pp. 74–77, Jun. 2015.
[12] K. Yamamoto, S. Yanagawa, K. Yamabuki, S. Sekioka, and S. Yokoyama, "Analytical Surveys of Transient and Frequency-Dependent Grounding Characteristics of a Wind Turbine Generator System on the Basis of Field Tests," IEEE Transactions on Power Delivery, vol. 25, no. 4, pp. 3035–3043, Oct. 2010.

[13] A. Sunjerga, Q. Li, D. Pojak, M. Rubinstein, F. Rachidi "Transient Impedance of Interconnected Wind Turbine Grounding Systems", 2018 26th International Conference on Software, Telecommunications and Computer Networks (SoftCOM)
[14] R. Alipio and S. Visacro, "Frequency dependence of soil parameters: Effect on the lightning response of grounding electrodes," IEEE Trans. Electromagn. Compat., vol. 55, no. 1, pp. 132–139, Feb. 2013.
[15] M. Akbari, K. Sheshyekani, and M. R. Alemi, "The effect of frequency dependence of soil electrical parameters on the lightning performance of grounding systems," IEEE Trans. Electromagn. Compat., vol. 55, no. 4, pp. 739–746, Aug. 2013.
[16] M. Mokhtari, Z. Abdul-Malek, and G. B. Gharehpetian, "A critical review on soil ionisation modelling for grounding electrodes," Archives of Electrical Engineering, vol. 65, no. 3, Jan. 2016.
[17] Markovski, B., Grcev, L., & Arnautovski-Toseva, V. (2012). Transient characteristics of wind turbine grounding. In 2012 International Conference on Lightning Protection (ICLP). IEEE. https://doi.org/10.1109/iclp.2012.6344413
[18] D. S. Gazzana, A. Smorgonskiy, N. Mora, A. Šunjerga, M. Rubinstein, and F. Rachidi, "An experimental field study of the grounding system response of tall wind turbines to impulse surges," Electric Power Systems Research, vol. 160, pp. 219–225, Jul. 2018.
[19] D. Cavka, D. Poljak, V. Doric, and R. Goic, "Transient analysis of grounding systems for wind turbines," Renewable Energy, vol. 43, pp. 284–291, Jul. 2012.
[20] B. Markovski, L. Grcev, and V. Arnautovski-Toseva, "Step and touch voltages near wind turbine grounding during lightning strokes," in International Symposium on Electromagnetic Compatibility - EMC EUROPE, 2012.
[21] G. C. Topp, J. L. Davis, and A. P. Annan, "Electromagnetic determination of soil water content: Measurements in coaxial transmission lines," Water Resources Research, vol. 16, no. 3, pp. 574–582, Jun. 1980.
[22] Roberta Porretta and Fabio Bianchi, "Profiles of relative permittivity and electrical conductivity from unsaturated soil water content models," Annals of Geophysics, vol. 59, no. 3, Jul. 2016.
[23] J. H. Scott, "Electrical and magnetic properties of rock and soil," Open-File Report. US Geological Survey, 1983.
[24] G. J. Burke, "Numerical Electromagnetics Code (NEC-4) – Method of Moments, Part II: Program Description – Theory", Lawrence Livermore National Laboratory, YCRL-MA-109338 PT. II. 1992.
[25] D. Poljak Advanced modeling in computational electromagnetic compatibility, N.J. : Wiley, 2007.
[26] A. Sunjerga et al., "Tower and Path-Dependent Voltage Effects on the Measurement of Grounding Impedance for Lightning Studies," IEEE Transactions on Electromagnetic Compatibility, pp. 1–10, 2018.
[27] S. Visacro, R. Alipio, M. H. Murta Vale, and C. Pereira, "The Response of Grounding Electrodes to Lightning Currents: The Effect of Frequency-Dependent Soil Resistivity and Permittivity," IEEE Transactions on Electromagnetic Compatibility, vol. 53, no. 2, pp. 401–406, May 2011
[28] C. L. Longmire and H. J. Longley. (1973). "Time domain treatment of media with frequency dependent parameters," Theoretical Notes 113, Defense Nuclear Agency, Santa Barbara, CA, USA [Online]. Available: https://www.ece.unm.edu/summa/notes/Theoretical.html
[29] R. C. Bigelow and W. R. Eberle, "Empirical predictive curves for resistivity and dielectric constant of earth materials: 100 Hz to 100 MHz," Open-File Report 83-911, U.S. Geological Survey, 1972.
[30] J. He, R. Zeng, and B. Zhang, Methodology and Technology for Power System Grounding. Singapore: Wiley, 2013, p. 35.
[31] D. Cavka, N. Mora, and F. Rachidi, "A Comparison of Frequency-Dependent Soil Models: Application to the Analysis of Grounding Systems," IEEE Transactions on Electromagnetic Compatibility, vol. 56, no. 1, pp. 177–187, Feb. 2014.
[32] M. A. Messier, "The propagation of an electromagnetic impulse through soil: Influence of frequency dependent parameters," Mission Res. Corp., Santa Barbara, CA, USA, Tech. Rep. MRC-N-415, 1980.

[33] R. Alipio and S. Visacro, “Modeling the Frequency Dependence of Electrical Parameters of Soil,” IEEE Transactions on Electromagnetic Compatibility, vol. 56, no. 5, pp. 1163–1171, Oct. 2014.
[34] F. Heidler, “Analytische Blitzstromfunktion zur LEMP- Berechnung,” in Proc. 18th Int. Conf. Lightning Protection, Munich, Sept. 16–20,1985, paper 1.9, pp. 63–66.
[35] F. Rachidi, W. Janischewskyj, A. M. Hussein, C. A. Nucci, S. Guerrieri, B. Kordi, and J. Chang, “Current and Electromagnetic Field Associated with Lightning–Return Strokes to Tall Towers”, IEEE Transactions on Electromagnetic Compatibility, Vol. 43, No. 3, 2001.
[36] Frigo, M., and S. G. Johnson. “FFTW: An Adaptive Software Architecture for the FFT.” Proceedings of the International Conference on Acoustics, Speech, and Signal Processing. Vol. 3, 1998, pp. 1381-1384.
[37] de Boor, Carl. A Practical Guide to Splines. Springer-Verlag, New York: 1978.
[38] K. Yamamoto and S. Sumi, “Transient grounding characteristics of a wind turbine foundation with grounding wires and plates,” in 2014 IEEE International Symposium on Electromagnetic Compatibility (EMC), 2014.